buildings

MDPI

Article

The Comparison of Code-Based and Empirical Seismic Fragility Curves of Steel and RC Buildings

Mahnoosh Biglari [1,*], Behrokh Hosseini Hashemi [2] and Antonio Formisano [3]

[1] Civil Engineering Department, School of Engineering, Razi University, Kermanshah P.O. Box 67149-67346, Iran
[2] Department of Structures, International Institute of Earthquake Engineering and Seismology (IIEES), Tehran P.O. Box 19537-14453, Iran; behrokh@iiees.ac.ir
[3] Department of Structures for Engineering and Architecture, School of Polytechnic and Basic Sciences, University of Naples Federico II, 80138 Naples, Italy; antoform@unina.it
* Correspondence: m.biglari@razi.ac.ir

Abstract: Seismic codes were developed to reduce the structural vulnerability and risk associated with earthquakes in earthquake-prone regions of the world. The effectiveness of the code in preventing damage is dependent on the performance level defined and the construction technology employed. The seismic fragility curves for two recent versions of the seismic code of Iran are determined by using the hybrid method. The probability of damage levels is visualized by these curves. To develop these curves, only the assumptions of the code are taken into account. These curves are compared with the empirical fragility of the recent devastating earthquake in Iran. The results indicate that, despite a similar probability of damage to the different seismic-resistant systems, steel-braced frames pose a greater risk of collapse. Concerning earthquake damage, the steel and RC moment-resisting frames have shown higher damage probability than expected from the code.

Keywords: capacity curves; fragility curves; code-based approach; steel and RC buildings; Iranian earthquake code

Citation: Biglari, M.; Hosseini Hashemi, B.; Formisano, A. The Comparison of Code-Based and Empirical Seismic Fragility Curves of Steel and RC Buildings. *Buildings* **2023**, *13*, 1361. https://doi.org/10.3390/buildings13061361

Academic Editors: Rajesh Rupakhety and Dipendra Gautam

Received: 23 April 2023
Revised: 15 May 2023
Accepted: 20 May 2023
Published: 23 May 2023

1. Introduction

Seismic regulations are developed to ensure that all buildings that are at risk of being damaged by an earthquake are safe. Meanwhile, economic prosperity and technological advancement in construction are expected to have an impact on seismic code performance. Seismic regulations generally aim to minimize casualties from each earthquake event.

Other factors, such as complexity and diversity of site stratification, the quality of materials used, design and execution errors, past seismic experience, and maintenance throughout the structures, are also factors that determine earthquake damage to structures. Despite all of the above, seismic codes for each building accept damage even when all the design rules have been observed. Recommended assessment methods offered by different seismic codes were investigated in [1]. They compared the fragility curves of existing low- to mid-rise RC buildings designed with four seismic codes of TEC-2007 [2], TBEC-2018 [3], EC8/3 [4], and ASCE 41-17 [5] and showed that different code methods give remarkably different damage estimations under similar seismic demand levels. However, implementing the code design rules reduces the damage rate.

The seismic fragility curves provide an estimate of the likelihood of reaching or exceeding a specific damage level at each acceleration level for different limit states. The research focus is on determining seismic fragility curves for constructed buildings, rather than relying on assumptions in seismic codes. There are several ways to calculate seismic fragility curves: empirical, analytical, expert judgment, or a hybrid method. To propose the empirical method, an extensive database of peak ground motion parameters is required. The database is primarily accessible through the collection of information from strong

earthquakes [6–9]. The empirical fragility curves are widely used in urban-scale seismic vulnerability assessment [10]. The analytical seismic fragility curves are developed by modeling and analyzing structures statically or dynamically. The ground motion records should exhibit a wide range of low to high PGA values in the dynamic analysis. During the pioneering research, incremental dynamic analysis methods were used by scaling a ground motion record to various peak accelerations [11]. Therefore, only the amplitude of the record changes, and other parameters such as frequency content and duration are not scaled. Other researchers used a set of unscaled natural ground motion records with a wide range of amplitudes for the dynamic analysis, e.g., [12]. In the absence of natural ground motion records corresponding to the seismo-tectonic conditions of a region, stochastic ground motion records have been used to propose probabilistic seismic fragility curves [13] and three-dimensional consistent hazard–fragility curves considering multiple capacity–demand uncertainties [14]. Modeling requires a good understanding of the material properties and geometry. Many researchers followed the analytical method for fragility curves, e.g., [15–18]. Expert judgment-based methods are based on human opinions and are used to replace the process of numerical modeling or observed data. However, this method should be verified by the observed data or analytical methods. The pioneer of this method was the Applied Technology Council (funded by the Federal Emergency Management Agency (FEMA)), as summarized in ATC-13 [19]. The hybrid method combines the analytical results with the empirical parameters to establish damage limit state definitions. The RISK-UE Project [20] employed this method to determine seismic fragility curves for the Unified Building Code [21].

This research utilizes hybrid fragility curves based on seismic code considerations, independent of earthquake-resistant configuration systems, retrofitting, and maintenance interventions. Therefore, seismic code users are informed of the code-based fragility curves used to evaluate the seismic vulnerability of the structure. This paper presents capacity and hybrid seismic fragility curves for residential buildings designed following Iranian seismic code IRSt2800 [22,23] based on the methodology presented in Figure 1. These curves are not included in seismic standards.

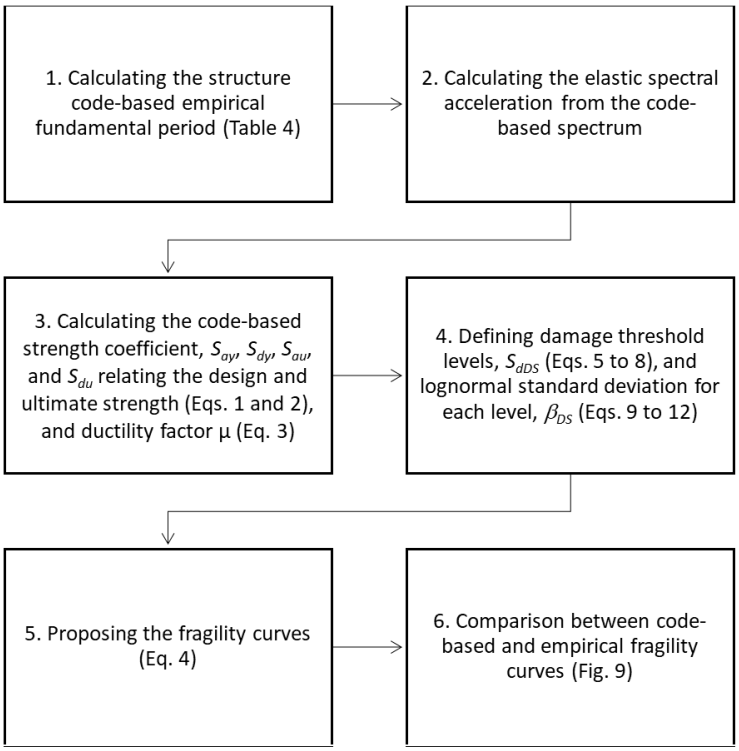

Figure 1. Methodology flowchart.

The Iranian seismic code has four versions. The third [22] and fourth [23] versions were considered in this research. These versions differ in the parameters used to calculate the base shear coefficient. The effects of these differences will be observed in the fragility curves later. The third version was considered because it was used for nine years to renovate residential, commercial, and administrative buildings in most major Iranian cities. Therefore, many existing steel (ST) buildings and reinforced concrete (RC) buildings were built based on this version of the seismic code. Furthermore, regarding the recent catastrophic earthquake in Iran, which occurred on 2017 November 12th in Sarpol-e-zahab, most of the exposed buildings were constructed according to the third version of the Iranian seismic code [22]. Therefore, the fragility curves of the third version can be compared with the existing empirical seismic fragility curves. Furthermore, the fragility curves provided in the fourth version of the seismic code [23], the most recent version, were utilized to assess the seismic performance of new buildings.

2. Building Typology and Damage Grades

The selected building typology matrix includes buildings built in the last 20 years based on the Iranian seismic code. The buildings' typologies are characterized by four factors: the seismic code, the building height, the construction frame material, and the seismic-resistant system.

Buildings are divided according to their seismic code version into two general categories: moderate code and high code. Buildings of the moderate code are constructed based on the third version (V3) of the Iranian seismic code [22], while high-code buildings are constructed based on the fourth (latest) version (V4) of the Iranian seismic code [23]. Tables 1 and 2 show the building typology matrices for moderate-code and high-code buildings, respectively. There are two sub-groups of buildings: low-rise (L) buildings (9 m in height or with three stories) and mid-rise (M) buildings (18 m in height or with six stories). In terms of construction materials, they are divided into two categories: steel (ST) buildings and reinforced concrete (RC) buildings. Each of these buildings has a different type based on the seismic-resistant system. Steel buildings are divided into three sub-categories: braced frames (including eccentric/concentric), moment-resisting frames (including special/intermediate), and a combination of moment-resisting and braced frames. The reinforced concrete buildings are divided into two sub-categories: moment-resisting frames (including special or intermediate) and a combination of moment-resisting frames and shear walls (including special or intermediate). The seismic-resistant system is named based on the seismic code system of Iran to be able to match with the code more easily. The last columns of Tables 1 and 2 contain the name of each building type. Subsequently, the studied structures are divided into 50 types (24 for moderate code and 26 for high code). For each of these 50 types, the fragility curves are presented based on the parameters introduced in the seismic code.

Table 1. The building typology matrix for moderate-code (V3) buildings.

Main Type	Description		Height	No. of Stories	Type Name
Steel (ST)	Braced frames	Eccentrically (EBF)	Low-rise (L)	3	B5-ST-L-V3
			Mid-rise (M)	6	B5-ST-M-V3
		Concentrically (CBF)	Low-rise (L)	3	B6-ST-L-V3
			Mid-rise (M)	6	B6-ST-M-V3
	Moment-resisting frame	Special (SMF)	Low-rise (L)	3	P4-ST-L-V3
			Mid-rise (M)	6	P4-ST-M-V3
		Intermediate (IMF)	Low-rise (L)	3	P5-ST-L-V3
			Mid-rise (M)	6	P5-ST-M-V3

Table 1. *Cont.*

Main Type	Description		Height	No. of Stories	Type Name
	Combination of moment-resisting frame and braced frame	SMF + EBF	Low-rise (L)	3	T4-ST-L-V3
			Mid-rise (M)	6	T4-ST-M-V3
		SMF + CBF	Low-rise (L)	3	T5-ST-L-V3
			Mid-rise (M)	6	T5-ST-M-V3
		IMF + EBF	Low-rise (L)	3	T6-ST-L-V3
			Mid-rise (M)	6	T6-ST-M-V3
		IMF + CBF	Low-rise (L)	3	T7-ST-L-V3
			Mid-rise (M)	6	T7-ST-M-V3
Reinforced concrete (RC)	Moment-resisting frame	Special (SMF)	Low-rise (L)	3	P1-RC-L-V3
			Mid-rise (M)	6	P1-RC-M-V3
		Intermediate (IMF)	Low-rise (L)	3	P2-RC-L-V3
			Mid-rise (M)	6	P2-RC-M-V3
	Combination of moment-resisting frame and RC shear wall	SMF + Special shear walls	Low-rise (L)	3	T1-RC-L-V3
			Mid-rise (M)	6	T1-RC-M-V3
		IMF + Intermediate shear walls	Low-rise (L)	3	T2-RC-L-V3
			Mid-rise (M)	6	T2-RC-M-V3

Table 2. The building typology matrix for high-code (V4) buildings.

Main Type	Description		Height	No. of Stories	Type Name
Steel (ST)	Braced frames	Eccentrically (EBF)	Low-rise (L)	3	B5-ST-L-V4
			Mid-rise (M)	6	B5-ST-M-V4
		Concentrically (CBF)	Low-rise (L)	3	B8-ST-L-V4
			Mid-rise (M)	6	B8-ST-M-V4
	Moment-resisting frame	Special (SMF)	Low-rise (L)	3	P4-ST-L-V4
			Mid-rise (M)	6	P4-ST-M-V4
		Intermediate (IMF)	Low-rise (L)	3	P5-ST-L-V4
			Mid-rise (M)	6	P5-ST-M-V4
	Combination of moment-resisting frame and braced frame	SMF + EBF	Low-rise (L)	3	T5-ST-L-V4
			Mid-rise (M)	6	T5-ST-M-V4
		IMF + EBF	Low-rise (L)	3	T6-ST-L-V4
			Mid-rise (M)	6	T6-ST-M-V4
		SMF + CBF	Low-rise (L)	3	T7-ST-L-V4
			Mid-rise (M)	6	T7-ST-M-V4
		IMF + CBF	Low-rise (L)	3	T8-ST-L-V4
			Mid-rise (M)	6	T8-ST-M-V4
Reinforced concrete (RC)	Moment-resisting frame	Special (SMF)	Low-rise (L)	3	P1-RC-L-V4
			Mid-rise (M)	6	P1-RC-M-V4
		Intermediate (IMF)	Low-rise (L)	3	P2-RC-L-V4
			Mid-rise (M)	6	P2-RC-M-V4

Table 2. *Cont.*

Main Type	Description		Height	No. of Stories	Type Name
	Combination of moment-resisting frame and RC shear wall	SMF + Special shear walls	Low-rise (L)	3	T1-RC-L-V4
			Mid-rise (M)	6	T1-RC-M-V4
		IMF + Special shear walls	Low-rise (L)	3	T2-RC-L-V4
			Mid-rise (M)	6	T2-RC-M-V4
		IMF + Intermediate shear walls	Low-rise (L)	3	T3-RC-L-V4
			Mid-rise (M)	6	T3-RC-M-V4

The ground type is assumed to be rocky (type I based on IRSt2800 [22,23]). Similar to the area affected by the Sarpol-e-zahab earthquake, the hazard zone is considered a high-risk area (peak ground acceleration of PGA = 0.3 g based on IRSt2800 [22,23]). The results are therefore comparable with the existing empirical fragility curves presented in [9].

Based on the LM2 methodology of the RISK-UE project [20], the damage state is assessed following the FEMA/NIBS [24] guidelines. It uses four labels of DS (S = 1 to 4) which distinguish the no-damage building state from D0 (Table 3).

Table 3. Damage grading description.

Damage Grade	Damage Grade Label	Structural Damage	Non-Structural Damage	Description
None	D0	No	No	No
Minor	D1	No	Slight	Fine cracks in plaster over frame members or in walls at the base. Fine cracks in partitions and infills.
Moderate	D2	Slight	Moderate	Cracks in columns and beams of frames and structural walls. Cracks in partition and infill walls; fall of brittle cladding and plaster. Falling mortar from the joints of wall panels.
Severe	D3	Moderate	Heavy	Cracks in columns and beam–column joints of frames at the base and joints of coupled walls. Spilling of concrete cover, buckling of reinforced rods. Large cracks in partition and infill walls, failure of individual infill panels.
Collapse	D4	Heavy and very heavy	Very heavy and total collapse	Large cracks in structural elements with compression failure of concrete and fracture of rebars; bond failure of beam-reinforced bars; tilting of columns. The collapse of either a few columns or a single upper floor. The collapse of the ground floor or parts (e.g., wings) of buildings.

3. Capacity Spectra

It is necessary to obtain capacity curves from the code parameters for each type of building to develop code-based seismic fragility curves. This method estimates the expected first-mode peak response of a building at a given demand. The first mode of vibration of buildings is assumed to be dominant. Iranian seismic code-based bilinear capacity curves are based on yield and ultimate structural strength levels. The values are obtained from the prescribed values of the code for each type of seismic-resistant system.

Equations (1) and (2) define the coordinates for the yield capacity and the ultimate capacity points of the capacity curves, respectively. From Fajfar [25], period and ductil-

ity are assumed, and spectral acceleration and displacement are all determined in these two equations for four unknown quantities in the force-based design method.

$$\text{Yield capacity point } (S_{ay}, S_{dy}): \begin{cases} S_{ay} = \Omega_0 \frac{C_s}{\alpha_1} g \\ S_{dy} = \frac{S_{ay}}{4\pi^2} T^2 = \Omega_0 \frac{C_s}{\alpha_1} \frac{T^2}{4\pi^2} g \end{cases} \quad (1)$$

$$\text{Ultimate capacity point } (S_{au}, S_{du}): \begin{cases} S_{au} = \lambda S_{ay} = \lambda \Omega_0 \frac{C_s}{\alpha_1} g \\ S_{du} = \lambda \mu S_{dy} = \lambda \mu \Omega_0 \frac{C_s}{\alpha_1} \frac{T^2}{4\pi^2} g \end{cases} \quad (2)$$

where S_{ay} and S_{au} are spectral acceleration for yield and ultimate points, respectively. S_{dy} and S_{du} are spectral displacements for yield and ultimate points, respectively. Cs is the base shear coefficient corresponding to the design strength of the first plastic hinge (Figure 2). According to the seismic code of Iran [22,23], Cs is the ratio of ground spectral acceleration from the standard design spectra of the code (Figure 3) and the code strength reduction factor, R (Table 4) (i.e., $Cs = S_{ag}/R$). The code recommends that this coefficient be multiplied by the coefficient of the importance of structures. This coefficient is equal to 1 for residential buildings considered in this research. Ω_0 is an over-strength factor equal to 2.8 for the V3 of [22] and 2 for the V4 of [23]. $\lambda = 1 + k_{pl}$ where k_{pl} is the slope of the plastic branch considered here based on expert judgment equal to 20%. α_1 is an effective mass coefficient that Freeman [26] suggested adopting as between 0.75 to 0.83 for most multi-story buildings. Milutinovic and Trendafiloski [27] estimated 0.71 to 0.73 for RC frame and RC dual-system buildings. Here, α_1 is considered equal to 0.75 and T is a typical elastic period of the building that may be estimated using empirically developed formulas from the code presented in Table 4 for various structural typologies. μ is the ductility demand calculated by bilinear Equation (3) (e.g., [28,29]) from the representation of the code strength reduction factor R.

$$\begin{cases} \mu = (R-1)\frac{T_C}{T} + 1 & T < T_C \\ \mu = R & T \geq T_C \end{cases} \quad (3)$$

where T_C is a characteristic period of the ground motion, typically defined as the corner period at the beginning of the constant velocity range. A typical value of T_C, for IRSt2800 [22,23] for a rocky site, is equal to 0.4 s.

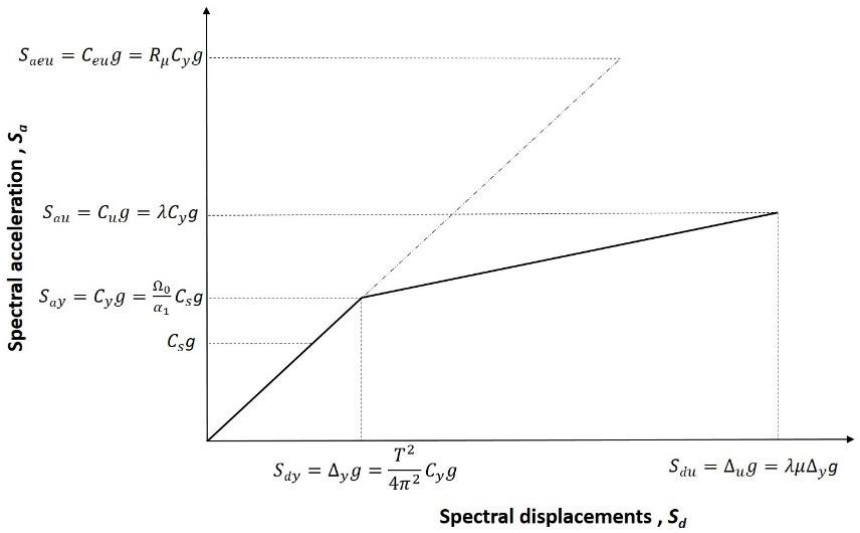

Figure 2. Bilinear idealization of capacity curve.

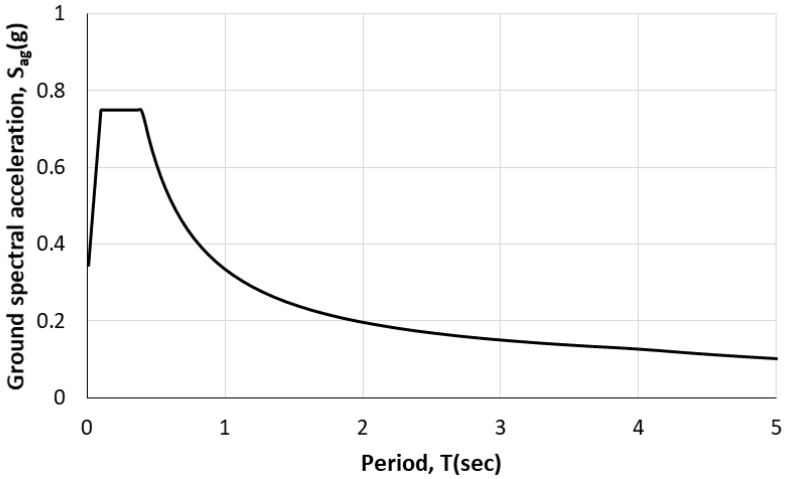

Figure 3. Standard design spectra of the codes [22,23] for a 475-year return period.

Table 4. Empirical formula for fundamental period of the building and the code strength reduction factor R of V3 [22] and V4 [23].

Typology		V3		V4	
		***T* (s)**	***R***	***T* (s)**	***R***
Steel	EBF	$0.05H^{0.75}$	7	$0.05H^{0.75}$	7
	CBF		6		5.5
	SMF	$0.08H^{0.75}$	10	$0.08H^{0.75}$	7.5
	IMF		7		5
	SMF + EBF	$0.05H^{0.75}$	10	$0.05H^{0.75}$	7.5
	SMF + CBF		9		7
	IMF + EBF		7		6
	IMF + CBF		7		6
Reinforced concrete	SMF	$0.07H^{0.75}$	10	$0.05H^{0.9}$	7.5
	IMF		7		5
	SMF + Special shear walls	$0.05H^{0.75}$	11	$0.05H^{0.75}$	7.5
	IMF + Special shear walls		-		6.5
	IMF + Intermediate shear walls		8		6

The capacity model parameters based on moderate code and high code for all 50 building typologies are presented in Tables 5 and 6, respectively. This presentation format of the demand spectrum is known as the acceleration–displacement response spectrum (ADRS) [30].

In both seismic codes, the capacity spectra for buildings with the same height show that steel moment-resisting frame buildings have the most significant spectral displacement (P4 and P5). Buildings with steel-braced frames (B5 and B8) have the lowest values of spectral displacement. However, values of spectral displacement in steel and RC combined frames are also close to those of steel-braced frames with a slight difference. The values presented in the capacity curves were determined by the parameters introduced in the seismic codes. If the drift of the floor surpasses the allowable value in the code, the designer will reduce the assumed ductility for the next attempt.

Table 5. Parameters of the capacity curves for moderate-code steel and RC buildings.

Building Typology	Yield Point		Ultimate Point	
	S_{dy} (cm)	S_{ay} (cm/s^2)	S_{du} (cm)	S_{au} (cm/s^2)
B5-ST-L-V3	0.94	549.36	11.54	659.23
B6-ST-L-V3	1.10	640.92	11.44	769.10
P4-ST-L-V3	1.68	384.55	20.20	461.46
P5-ST-L-V3	2.40	549.36	20.20	659.23
T4-ST-L-V3	0.66	384.55	11.72	461.46
T5-ST-L-V3	0.73	427.28	11.67	512.74
T6&T7-ST-L-V3	0.94	549.36	11.54	659.23
P1-RC-L-V3	1.29	384.55	16.85	461.46
P2-RC-L-V3	1.84	549.36	16.79	659.23
T1-RC-L-V3	0.60	349.59	11.76	419.51
T2-RC-L-V3	0.82	480.69	11.61	576.83
B5-ST-M-V3	2.66	549.36	22.32	659.23
B6-ST-M-V3	3.10	640.92	22.32	769.10
P4-ST-M-V3	3.28	265.03	39.37	318.04
P5-ST-M-V3	4.69	378.62	39.37	454.34
T4-ST-M-V3	1.86	384.55	22.32	461.46
T5-ST-M-V3	2.07	427.28	22.32	512.74
T6&T7-ST-M-V3	2.66	549.36	22.32	659.23
P1-RC-M-V3	2.75	289.71	32.95	347.65
P2-RC-M-V3	3.92	413.87	32.95	496.64
T1-RC-M-V3	1.79	369.29	23.57	443.15
T2-RC-M-V3	2.46	507.77	23.57	609.32

Table 6. Parameters of the capacity curves for high-code steel and RC buildings.

Building Typology	Yield Point		Ultimate Point	
	S_{dy} (cm)	S_{ay} (g)	S_{du} (cm)	S_{au} (g)
B5-ST-L-V4	0.48	280.29	5.89	336.34
B8-ST-L-V4	0.61	356.73	5.80	428.07
P4-ST-L-V4	1.72	392.40	15.46	470.88
P5-ST-L-V4	2.58	588.60	15.46	706.32
T5-ST-L-V4	0.56	327.00	7.38	392.40
T7-ST-L-V4	0.60	350.36	7.36	420.43
T6&T8-ST-L-V4	0.70	408.75	7.29	490.50
P1-RC-L-V4	1.30	392.40	12.76	470.88
P2-RC-L-V4	1.94	588.60	12.67	706.32
T1-RC-L-V4	0.59	345.42	7.80	414.51
T2-RC-L-V4	0.68	398.56	7.74	478.28
T3-RC-L-V4	0.74	431.78	7.71	518.13
B5-ST-M-V4	1.35	280.29	11.39	336.34
B8-ST-M-V4	1.72	356.73	11.39	428.07

Table 6. *Cont.*

Building Typology	Yield Point		Ultimate Point	
	S_{dy} (cm)	S_{ay} (g)	S_{du} (cm)	S_{au} (g)
P4-ST-M-V4	2.78	224.51	25.02	269.42
P5-ST-M-V4	4.17	336.77	25.02	404.13
T5-ST-M-V4	1.58	327.00	14.23	392.40
T7-ST-M-V4	1.69	350.36	14.23	420.43
T6&T8-ST-M-V4	1.98	408.75	14.23	490.50
P1-RC-M-V4	2.68	232.85	24.12	279.42
P2-RC-M-V4	4.02	349.27	24.12	419.13
T1-RC-M-V4	1.67	345.42	15.03	414.51
T2-RC-M-V4	1.93	398.56	15.03	478.28
T3-RC-M-V4	1.97	408.21	14.21	489.85

4. Fragility Curves

Seismic fragility curves indicate the probability of $P[\mathrm{DS} \mid S_d]$ reaching or exceeding a specific damage state DS under a given ground motion parameter (e.g., peak ground acceleration *PGA*, spectrum displacement S_d, intensity *I*). The LM2 hybrid method introduced in RISK-UE [20] was employed to extract the seismic fragility curves for a given spectrum displacement S_d, as defined in Equation (4) [31]:

$$P[DS|S_d] = \Phi\left[\frac{1}{\beta_{DS}} \ln\left(\frac{S_d}{S_{dDS}}\right)\right] \quad (4)$$

where Φ is the standard normal cumulative distribution function, $S_{d\mathrm{DS}}$ is the median value of spectral displacement at which the building reaches the threshold of the damage state, DS, and β_{DS} is the lognormal standard deviation of spectral displacement for the damage state DS.

The median values introduced by LM2 of the RISK-UE method [20] for damage limit states, depending on S_{dy} and S_{du}, are used in Equations (5)–(8):

$$S_{dD1} = 0.7S_{dy} \quad (5)$$

$$S_{dD2} = S_{dy} \quad (6)$$

$$S_{dD3} = S_{dy} + 0.25(S_{du} - S_{dy}) \quad (7)$$

$$S_{dD4} = S_{du} \quad (8)$$

The lognormal standard deviation of spectral displacement for damage state DS presented in LM2 of the RISK-UE method [20] as a function of ductility μ is as in Equations (9)–(12):

$$\beta_{D1} = 0.25 + 0.07 \ln(\mu) \quad (9)$$

$$\beta_{D2} = 0.20 + 0.18 \ln(\mu) \quad (10)$$

$$\beta_{D3} = 0.10 + 0.4 \ln(\mu) \quad (11)$$

$$\beta_{D4} = 0.15 + 0.5\ln(\mu) \quad (12)$$

Tables 7 and 8 show the parameters of hybrid fragility curves for the moderate-code buildings and the high-code buildings, respectively. Likewise, spectral displacement curves corresponding to moderate-code low-rise, high-code low-rise, and high-code mid-rise buildings are shown in Figures 4–7.

Table 7. Parameters of fragility curves for moderate-code steel and RC buildings.

Building Properties		Spectral Displacements, S_d (cm)							
Typology	Height (m)	D1		D2		D3		D4	
		Median	Beta	Median	Beta	Median	Beta	Median	Beta
B5-ST-L-V3	9	0.66	0.41	0.94	0.62	3.59	1.03	11.54	1.31
B6-ST-L-V3		0.77	0.40	1.10	0.59	3.68	0.96	11.44	1.23
P4-ST-L-V3		1.18	0.41	1.68	0.61	6.31	1.02	20.20	1.30
P5-ST-L-V3		1.68	0.39	2.40	0.55	6.85	0.88	20.20	1.12
T4-ST-L-V3		0.46	0.44	0.66	0.69	3.42	1.18	11.72	1.50
T5-ST-L-V3		0.51	0.43	0.73	0.67	3.47	1.14	11.67	1.44
T6&T7-ST-L-V3		0.66	0.41	0.94	0.62	3.59	1.03	11.54	1.31
P1-RC-L-V3		0.90	0.42	1.29	0.63	5.18	1.05	16.85	1.34
P2-RC-L-V3		1.29	0.39	1.84	0.56	5.58	0.91	16.79	1.16
T1-RC-L-V3		0.42	0.45	0.60	0.70	3.39	1.22	11.76	1.55
T2-RC-L-V3		0.57	0.42	0.82	0.64	3.52	1.09	11.61	1.38
B5-ST-M-V3	18	1.86	0.39	2.66	0.55	7.57	0.88	22.31	1.12
B6-ST-M-V3		2.17	0.37	3.10	0.52	7.90	0.82	22.32	1.05
P4-ST-M-V3		2.30	0.41	3.28	0.61	12.30	1.02	39.37	1.30
P5-ST-M-V3		3.28	0.39	4.69	0.55	13.36	0.88	39.37	1.12
T4-ST-M-V3		1.30	0.41	1.86	0.61	6.97	1.02	22.32	1.30
T5-ST-M-V3		1.45	0.40	2.07	0.59	7.13	0.98	22.32	1.25
T6&T7-ST-M-V3		1.86	0.39	2.66	0.55	7.57	0.88	22.32	1.12
P1-RC-M-V3		1.92	0.41	2.75	0.61	10.30	1.02	32.95	1.30
P2-RC-M-V3		2.75	0.39	3.92	0.55	11.18	0.88	32.95	1.12
T1-RC-M-V3		1.25	0.42	1.79	0.63	7.23	1.06	23.57	1.35
T2-RC-M-V3		1.72	0.40	2.45	0.57	7.73	0.93	23.57	1.19

Table 8. Parameters of fragility curves for high-code steel and RC buildings.

Building Properties		Spectral Displacements, S_d (cm)							
Typology	Height (m)	D1		D2		D3		D4	
		Median	Beta	Median	Beta	Median	Beta	Median	Beta
B5-ST-L-V4	9	0.33	0.41	0.48	0.62	1.83	1.03	5.89	1.31
B8-ST-L-V4		0.43	0.39	0.618	0.57	1.91	0.93	5.80	1.18
P4-ST-L-V4		1.20	0.39	1.72	0.56	5.15	0.91	15.46	1.16
P5-ST-L-V4		1.80	0.36	2.58	0.49	5.80	0.74	15.46	0.95
T5-ST-L-V4		0.39	0.42	0.56	0.63	2.27	1.06	7.38	1.35

Table 8. *Cont.*

Building Properties		Spectral Displacements, S_d (cm)							
Typology	Height (m)	D1		D2		D3		D4	
		Median	Beta	Median	Beta	Median	Beta	Median	Beta
T7-ST-L-V4		0.42	0.41	0.60	0.62	2.29	1.03	7.36	1.31
T6&T8-ST-L-V4		0.49	0.40	0.70	0.59	2.35	0.96	7.29	1.23
P1-RC-L-V4		0.91	0.40	1.30	0.58	4.16	0.94	12.76	1.20
P2-RC-L-V4		1.36	0.37	1.94	0.50	4.63	0.78	12.67	1.00
T1-RC-L-V4		0.41	0.42	0.59	0.63	2.39	1.06	7.80	1.35
T2-RC-L-V4		0.48	0.41	0.68	0.60	2.45	1.00	7.74	1.27
T3-RC-L-V4		0.52	0.40	0.74	0.59	2.48	0.96	7.71	1.23
B5-ST-M-V4	18	0.95	0.39	1.35	0.55	3.86	0.88	11.39	1.12
B8-ST-M-V4		1.21	0.37	1.72	0.51	4.14	0.78	11.39	1.00
P4-ST-M-V4		1.95	0.39	2.78	0.56	8.34	0.91	25.01	1.16
P5-ST-M-V4		2.92	0.36	4.17	0.49	9.38	0.74	25.02	0.95
T5-ST-M-V4		1.11	0.39	1.58	0.56	4.74	0.91	14.23	1.16
T7-ST-M-V4		1.186	0.39	1.69	0.55	4.83	0.88	14.23	1.12
T6&T8-ST-M-V4		1.38	0.37	1.98	0.52	5.04	0.82	14.23	1.05
P1-RC-M-V4		1.88	0.39	2.68	0.56	8.04	0.91	24.12	1.16
P2-RC-M-V4		2.81	0.36	4.02	0.49	9.04	0.74	24.12	0.95
T1-RC-M-V4		1.17	0.39	1.67	0.56	5.01	0.91	15.03	1.16
T2-RC-M-V4		1.35	0.38	1.93	0.54	5.20	0.85	15.03	1.09
T3-RC-M-V4		1.38	0.37	1.97	0.52	5.03	0.82	14.21	1.05

For an elastic system with a single degree of freedom, the spectral acceleration S_a associated with the first mode-dominated period T is converted into the corresponding spectral displacement S_d, as shown in Equation (13):

$$S_d(T) = \frac{S_a(T)}{4\pi^2} T^2 \tag{13}$$

The corresponding fragility curves can be proposed in terms of spectral acceleration and damage discrete distribution. Figure 8 shows the fragility curves and damage distribution for high-code mid-rise buildings at S_a = 300 cm/s^2 (high relative seismic hazard zone). This shows the accepted damage by the IRSt2800 seismic code [23] for mid-height engineered buildings.

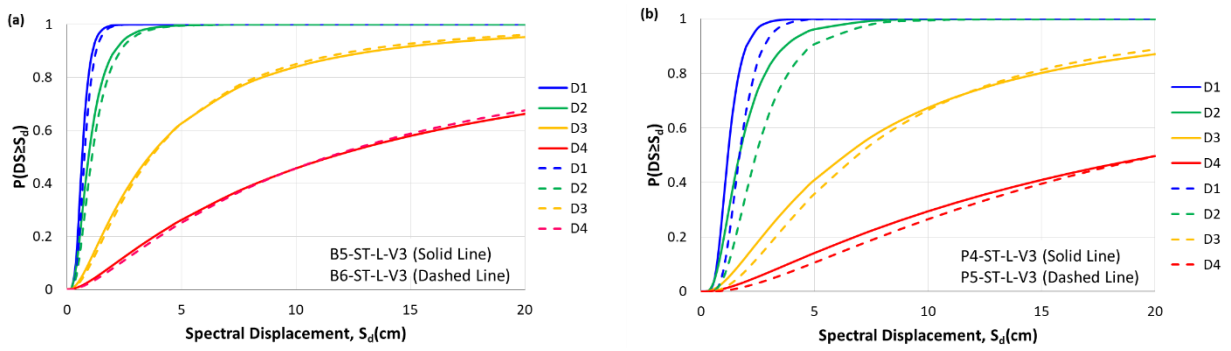

Figure 4. *Cont.*

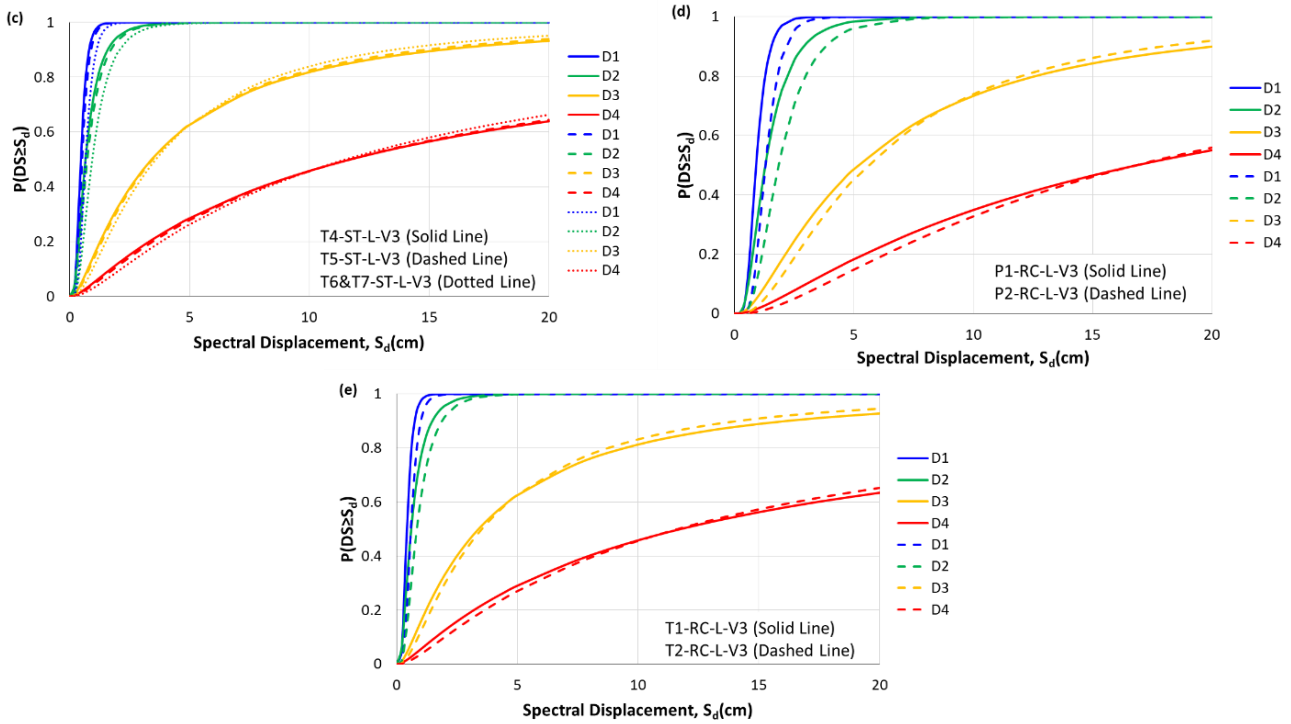

Figure 4. Fragility curves for moderate-code low-rise (9 m tall) steel and RC buildings: (**a**) steel-braced frame, (**b**) steel moment-resisting frame, (**c**) combination of moment-resisting frame and braced frame, (**d**) RC moment frame, and (**e**) combination of moment-resisting frame and RC shear wall.

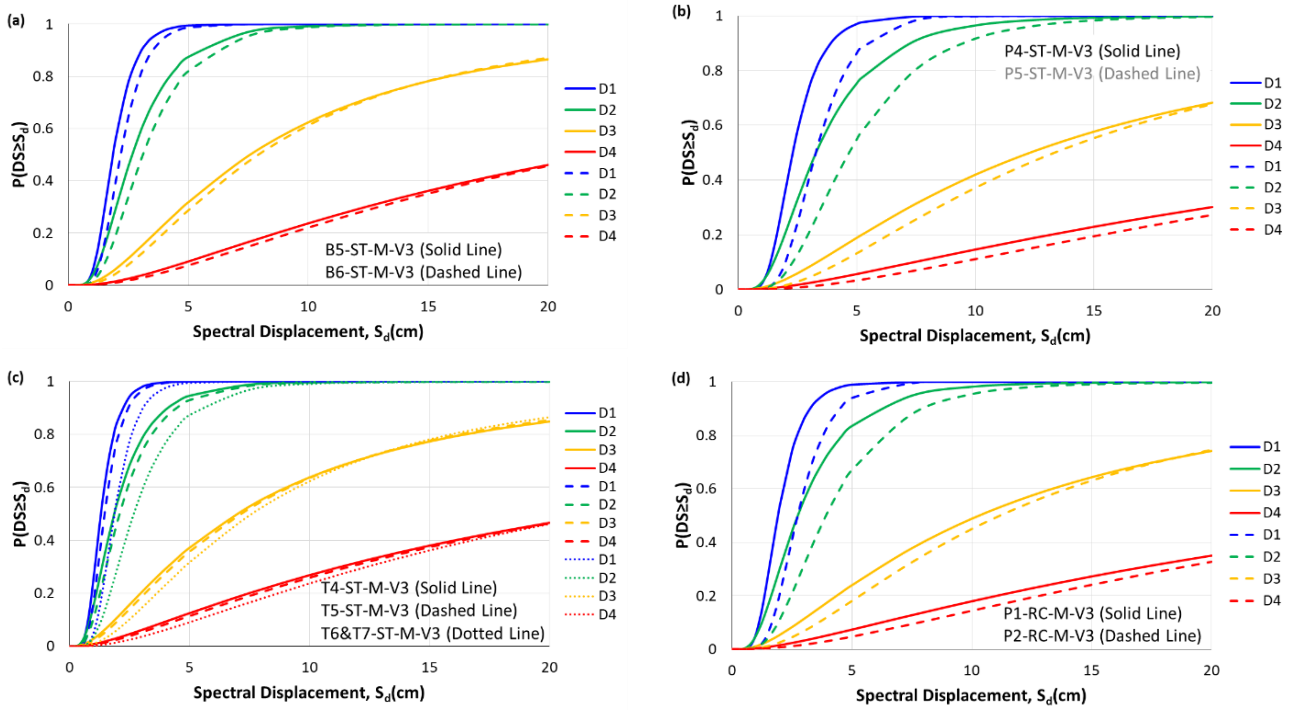

Figure 5. *Cont.*

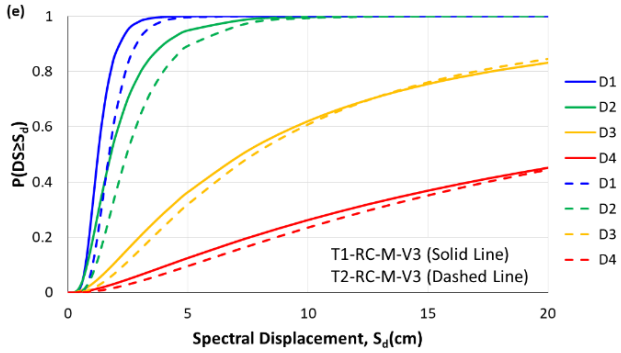

Figure 5. Fragility curves for moderate-code mid-rise (18 m tall) steel and RC buildings: (**a**) steel-braced frame, (**b**) steel moment-resisting frame, (**c**) combination of moment-resisting frame and braced frame, (**d**) RC moment frame, and (**e**) combination of moment-resisting frame and RC shear wall.

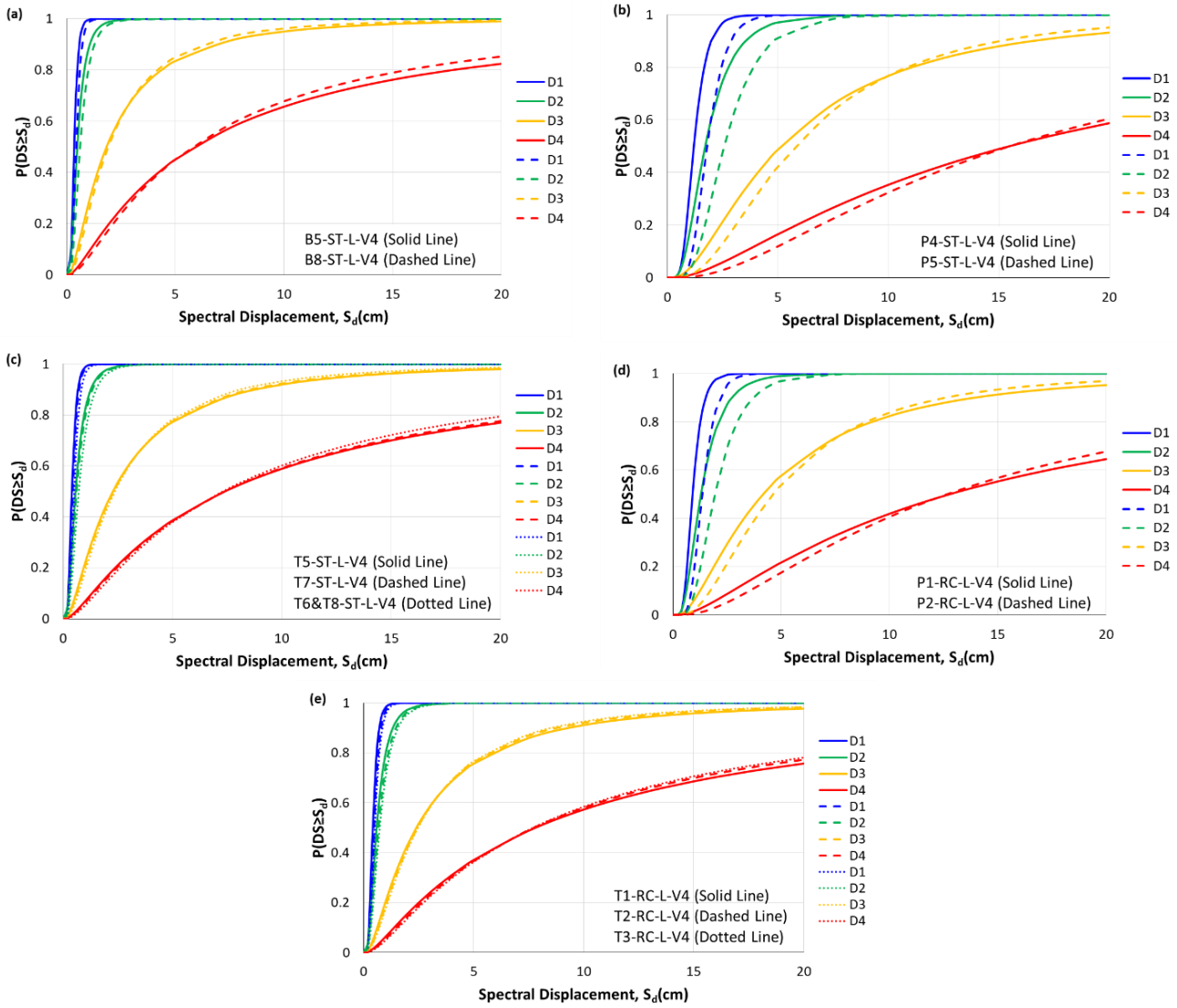

Figure 6. Fragility curves for high-code low-rise (9 m tall) steel and RC buildings: (**a**) steel-braced frame, (**b**) steel moment-resisting frame, (**c**) combination of moment-resisting frame and braced frame, (**d**) RC moment frame, and (**e**) combination of moment-resisting frame and RC shear wall.

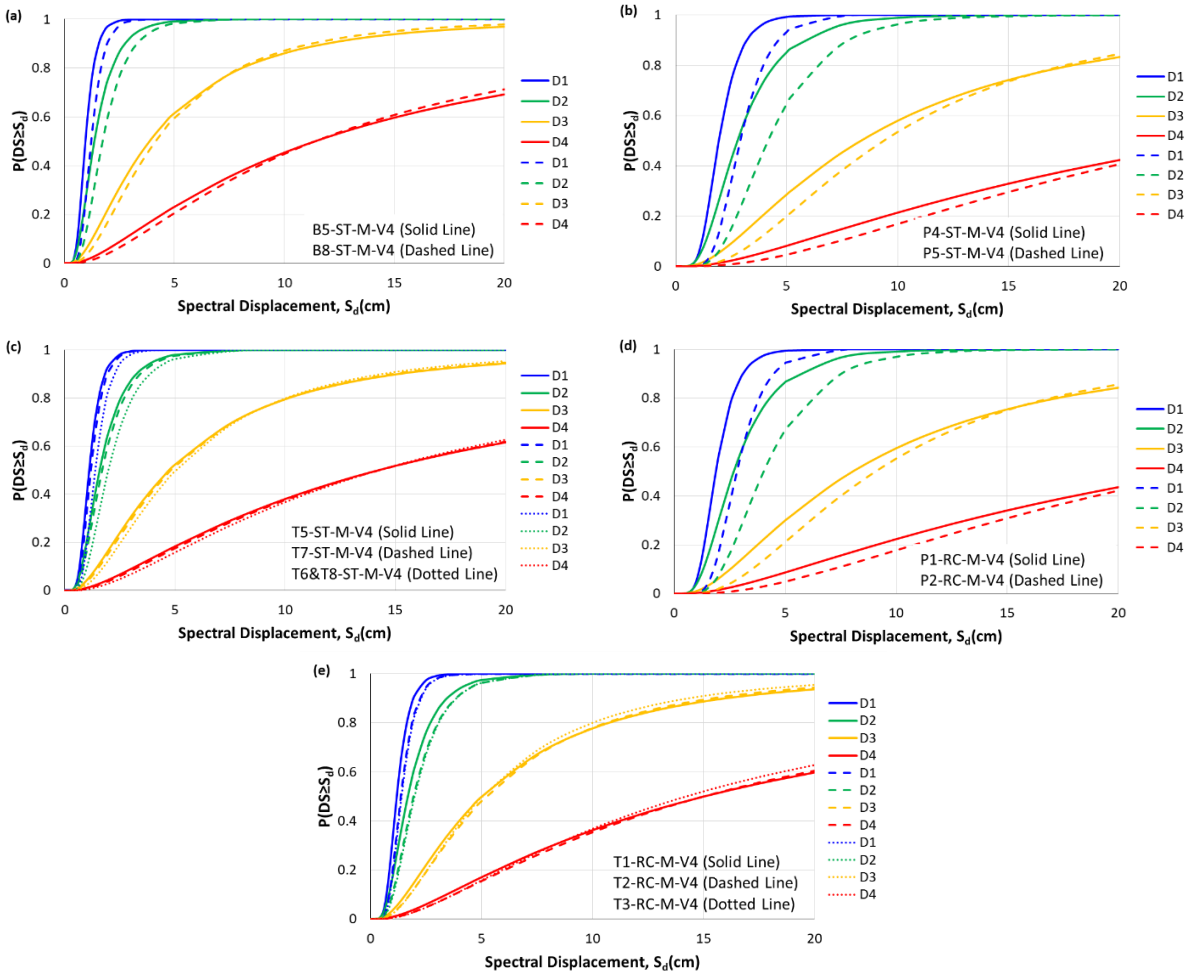

Figure 7. Fragility curves for high-code mid-rise (18 m tall) steel and RC buildings: (**a**) steel-braced frame, (**b**) steel moment-resisting frame, (**c**) combination of moment-resisting frame and braced frame, (**d**) RC moment frame, and (**e**) combination of moment-resisting frame and RC shear wall.

Different types of damage probability curves were evaluated by comparing their D4 damage level (collapse). For the low-rise and mid-rise buildings of the third version of the code, the highest probability of D4 damage in constant spectral displacement is related to the steel-braced frames and the combined steel and RC frames (Figure 4a,c,e and Figure 5a,c,e). However, according to the assumptions of the fourth version of the code, steel-braced frame buildings (Figures 6a and 7a) have the highest probability of D4-level damage in constant spectral displacement. Furthermore, the steel moment-resisting frame building type has the lowest probability of D4 damage in constant spectral displacement in both code versions and heights (Figures 4b, 5b, 6b and 7b).

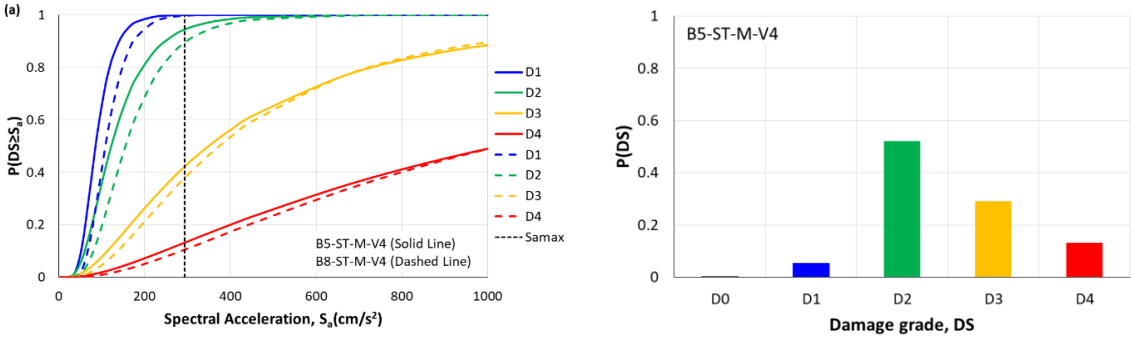

Figure 8. *Cont.*

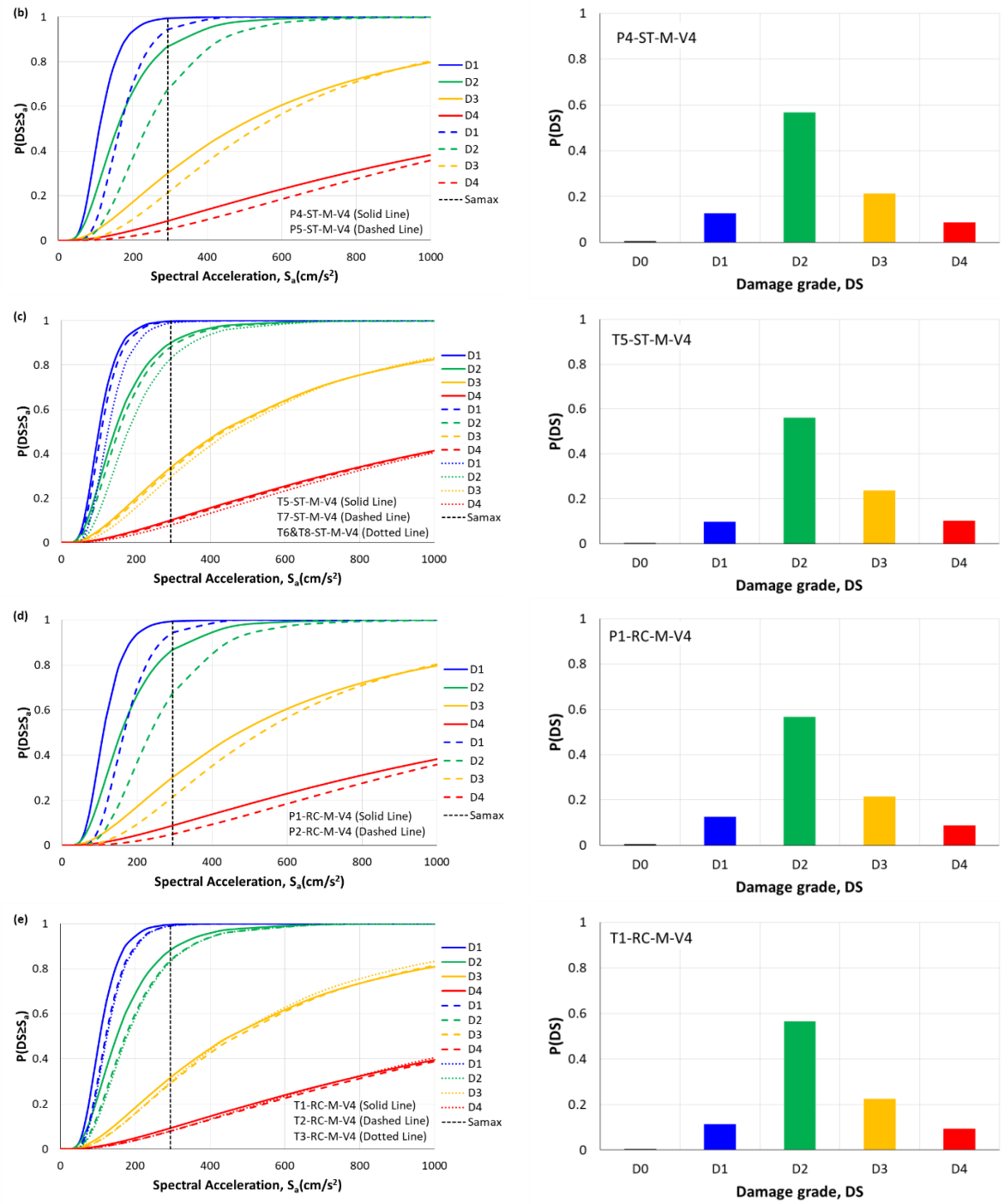

Figure 8. Fragility curves in terms of spectral acceleration and the discrete damage distribution referring to S_a = 300 cm/s^2 for high-code mid-rise (18 m tall) steel and RC buildings: (**a**) steel-braced frame, (**b**) steel moment-resisting frame, (**c**) combination of moment-resisting frame and braced frame, (**d**) RC moment frame, and (**e**) combination of moment-resisting frame and RC shear wall.

The results of the discrete damage distribution at constant spectral acceleration in mid-rise buildings of the fourth version of the code show that although the damage of different types is close at each level, the probability of D4 damage is slightly higher in the steel-braced frame. As shown in Figure 8, at a constant spectral acceleration of 0.3 g for different systems, the damage probability for D1 is about 5% to 13%, that of D2 is about 52% to 57%, that of D3 is about 21% to 29%, and that of D4 is estimated at 9% to 13%.

5. Comparison with Empirical Fragility Curves

The proposed code-based fragility curves (solid lines) are compared to the empirical fragility curves proposed in [9] (dashed lines) for buildings with the same seismic-resistant system, that were damaged during the 2017 Sarpol-e-zahab earthquake, in Figure 9. The proposed empirical fragility curves, based on the beta distribution of collected data, are regenerated to facilitate better comparisons since the empirical fragility curves are based on five levels of damage (D1 to D5) for LM1 of the RISK-UE method (Milutinovic and Trendafiloski, 2003). To achieve this, we assume that the D4 and D5 damage grades for LM1 of RISK-UE [20] will be the same as the collapse level (or D4 damage level) of LM2 of the method, based on the damage scale correlation of LM2 of the RISK-UE method [20]. It is also important to note that the curves at low spectral accelerations do not match up because the probability distribution functions are different (i.e., the beta distribution for the empirical fragility curves and the normal distribution for the code-based fragility curves). Furthermore, the height of the structures in the database of empirical fragility curves was not necessarily 18 m. According to a previous study [32] the demand estimation approaches can affect the performance of structures as well as the capacity estimation methods. Therefore, the observed discrepancies may also be attributed to assumptions underlying capacity and demand determinations.

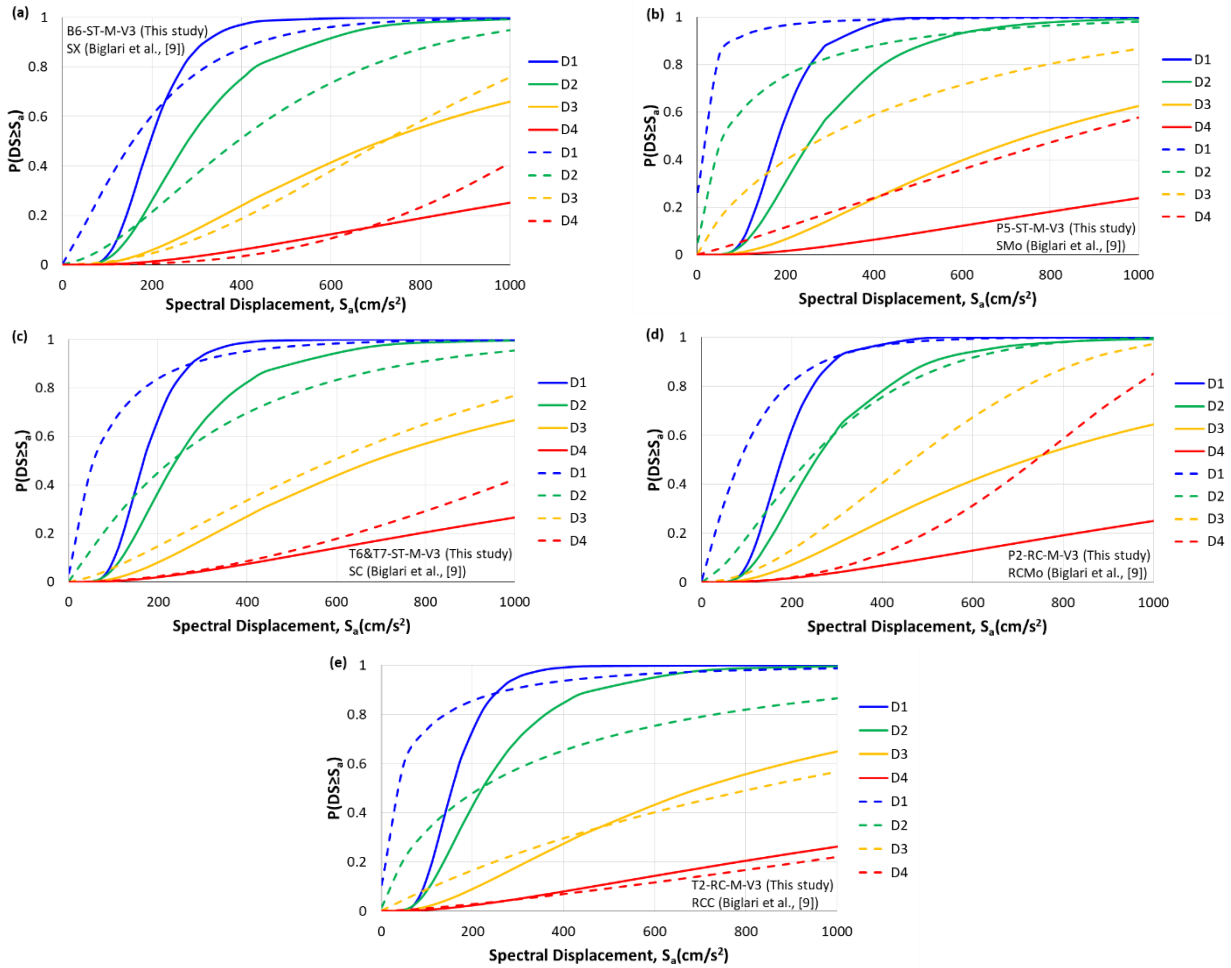

Figure 9. Comparison between moderate-code fragility curves proposed herein (solid line) and the empirical fragility curves developed by Biglari et al. [9] (dashed line) in terms of PGA for steel and RC buildings: (**a**) steel-braced frame, (**b**) steel moment-resisting frame, (**c**) combination of moment-resisting frame and braced frame, (**d**) RC moment frame, and (**e**) combination of moment-resisting frame and RC shear wall.

The results show that the damage probability at a high damage level (i.e., D4) in the real condition is higher than what the seismic code would expect. This poor performance is due to weaknesses in construction technologies and materials, as well as neglect of maintenance of structures. In RC buildings with a combination of moment-resisting frames and RC shear walls (Figure 9e) and steel-braced frames (Figure 9a), this difference is less than in the other seismic-resistant systems. This shows that these types of seismic-resistant systems work better with construction technologies in Iran. In the meantime, buildings with steel and RC moment frames (Figure 9b,d) have greater inconsistencies with the probability of code-expected damage. It is recommended to increase the technical controls of these buildings due to the increased demand for this seismic-resistant system in Iran.

6. Conclusions

The default values in seismic codes can be seen as a fragility curve, which gives seismic code developers a visual way to understand the seismic performance of different buildings and adjust them to meet real social and economic needs. These curves also help to plan seismic risk mitigation interventions for new code-based buildings, which are generally assumed to be invulnerable. This is specifically a comparison of codes and other parameters, such as the quality of materials, the construction methodology, the supervision of construction, and the maintenance during operation, which are other influential factors that will control the final seismic behavior of the structure.

The methodology employed in this study relies exclusively on the assumptions contained in the two latest Iranian seismic codes. These pure code-based seismic fragility curves have not been proposed to date. However, it is essential to consider the possibility of simulated damage in seismic codes. The limitation of this method is that it ignores design changes during deformation control. This issue occurs mostly with tall structures, and this effect cannot be considered in this method.

These two versions of the seismic design code recommended values for the minimum amount of nonlinear deformation and, therefore, the ductility factor for steel buildings with braced frames. However, steel buildings with special moment-resisting frames had the highest seismic capacity. Furthermore, the hybrid fragility curves for all typologies of the studied buildings were proposed. Seismic fragility curves are useful for figuring out how good codes are and how strong they are. These curves are not presented in seismic codes. Upon comparing the fragility curves of the third and fourth editions of the seismic code of Iran, it was found that the severe damage probability (D4) of the fourth version is higher than that of the third version. This comparison used a similar approach and only considered the assumptions included in the standard. The curves showed that steel buildings with braced frames had the highest probability of collapsing at constant spectral displacement, and steel buildings with moment-resistant frames had the lowest probability. Steel-braced frame buildings have the highest collapse probability in constant spectral acceleration among mid-rise buildings.

A comparison of results with empirical values showed that the steel-braced frames and RC buildings with a combination of moment-resisting frames and RC shear walls are more compatible with construction technologies in Iran. However, the steel and RC moment frames of buildings are incompatible. It is recommended to increase the technical controls on these buildings.

Determining these curves for other seismic codes and consciously changing the seismic codes could reduce the probability of D3 and D4 damage and, consequently, reduce the vulnerability of newly built structures. Further investigation is needed to find the most effective seismic code parameters to reduce the probability of high damage levels.

Author Contributions: Conceptualization, M.B.; methodology, M.B., B.H.H. and A.F.; software, M.B.; validation, M.B. and B.H.H.; formal analysis, M.B.; investigation, M.B.; resources, M.B.; writing—original draft preparation, M.B.; writing—review and editing, M.B., B.H.H. and A.F.; visualization, M.B.; supervision, M.B., B.H.H. and A.F.; project administration, M.B. All authors have read and agreed to the published version of the manuscript.

Funding: This research received no external funding.

Data Availability Statement: The text included all the presented research data.

Conflicts of Interest: The authors declare no conflict of interest.

References

1. Karakas, C.C.; Palanci, M.; Senel, S.M. Fragility based evaluation of different code based assessment approaches for the performance estimation of existing buildings. *Bull. Earthq. Eng.* **2022**, *20*, 1685–1716. [CrossRef]
2. Ministry of Public Works and Settlement of Turkey. *TEC 2007, Specification for Buildings to be Built in Seismic Zones*; Ministry of Public Works and Settlement of Turkey: Ankara, Turkey, 2007.
3. Disaster and Emergency Management Presidency of Turkey. *TBEC 2018, Turkey Earthquake Building Regulations*; Disaster and Emergency Management Presidency of Turkey: Ankara, Turkey, 2018.
4. CEN. *Eurocode 8: Design of Structures for Earthquake Resistance—Part 3: Assessment and Retrofitting of Buildings*; CEN: Brussels, Belgium, 2005.
5. American Society of Civil Engineers. *ASCE 41-17, Seismic Evaluation and Retrofit of Existing Buildings*; American Society of Civil Engineers: Reston, VA, USA, 2017.
6. Omidvar, B.; Gatmiri, B.; Derakhshan, S. Experimental vulnerability curves for the residential buildings of Iran. *Nat. Hazards* **2011**, *60*, 345–365. [CrossRef]
7. Del Gaudio, C.; De Martino, G.; Di Ludovico, M.; Manfredi, G.; Prota, A.; Ricci, P.; Verderame, G.M. Empirical fragility curves from damage data on RC buildings after the 2009 L'Aquila earthquake. *Bull. Earthq. Eng.* **2017**, *15*, 1425–1450. [CrossRef]
8. Gautam, D.; Fabbrocino, G.; de Magistris, F.S. Derive empirical fragility functions for Nepali residential buildings. *Eng. Struct.* **2018**, *171*, 617–628. [CrossRef]
9. Biglari, M.; Formisano, A.; Hashemi, B.H. Empirical fragility curves of engineered steel and RC residential buildings after Mw 7.3 2017 Sarpol-e-zahab earthquake. *Bull. Earthq. Eng.* **2021**, *19*, 2671–2689. [CrossRef]
10. Biglari, M.; Formisano, A. Urban seismic scenario-based risk analysis using empirical fragility curves for Kerendegharb after Mw 7.3, 2017 Iran earthquake. *Bull. Earthq. Eng.* **2022**, *20*, 6487–6503. [CrossRef]
11. Vamvatsikos, D.; Cornell, C.A. Incremental dynamic analysis. *Earthq. Eng. Struct. Dyn.* **2001**, *31*, 491–514. [CrossRef]
12. Réveillère, A.; Gehl, P.; Seyedi, D.; Modaressi, H. Development of seismic fragility curves for damaged reinforced concrete structures. In Proceedings of the 15th World Conference on Earthquake Engineering, Lisboa, Portugal, 24–28 September 2012; p. 999.
13. Cao, X.-Y.; Feng, D.-C.; Li, Y. Assessment of various seismic fragility analysis approaches for structures excited by non-stationary stochastic ground motions. *Mech. Syst. Signal Process.* **2023**, *186*, 109838. [CrossRef]
14. Cao, X.-Y.; Feng, D.-C.; Beer, M. Consistent seismic hazard and fragility analysis considering combined capacity-demand uncertainties via probability density evolution method. *Struct. Saf.* **2023**, *103*, 102330. [CrossRef]
15. Kappos, A.J.; Panagopoulos, G.; Panagiotopoulos, C.; Penelis, G. A hybrid method for the vulnerability assessment of R/C and URM buildings. *Bull. Earthq. Eng.* **2006**, *4*, 391–413. [CrossRef]
16. D'Ayala, D.; Meslem, A.; Vamvatsikos, D.; Porter, K.; Rossetto, T.; Crowley, H.; Silva, V. *Guidelines for Analytical Vulnerability Assessment of Low-Mid-Rise Buildings—Methodology*; Vulnerability Global Component Project; GEM Foundation: Pavia, Italy, 2014.
17. Simoncelli, M.; Aloisio, A.; Zucca, M.; Venturi, G.; Alaggio, R. Intensity and location of corrosion on the reliability of a steel bridge. *J. Constr. Steel Res.* **2023**, *206*, 107937. [CrossRef]
18. Suzuki, A.; Iervolino, I. Seismic Fragility of Code-conforming Italian Buildings Based on SDoF Approximation. *J. Earthq. Eng.* **2019**, *25*, 2873–2907. [CrossRef]
19. Applied Technology Council (ATC). *Earthquake Damage Evaluation Data for California, ATC-13*; Applied Technology Council (ATC): Redwood, CA, USA, 1985.
20. Milutinovic, Z.V.; Trendafiloski, G.S. *RISK-UE. An Advanced Approach to Earthquake Risk Scenarios with Applications to Different European Towns*; WP4: Vulnerability of Current Buildings; European Commission: Brussels, Belgium, 2004.
21. International Conference of Building Officials (ICBO). *Uniform Building Code*; International Conference of Building Officials (ICBO): Whittier, CA, USA, 1994.
22. Building and Housing Research Center. *IRSt2800, Iranian Code of Practice for Seismic Resistant Design of Buildings*, 3rd ed.; Building and Housing Research Center: Tehran, Iran, 2005.
23. Building and Housing Research Center. *IRSt2800, Iranian Code of Practice for Seismic Resistant Design of Buildings*, 4th ed.; Building and Housing Research Center: Tehran, Iran, 2014.
24. FEMA/NIBS. *HAZUS—Earthquake Loss Estimation Methodology*; Department of Homeland Security Federal Emergency Management Agency Mitigation Division: Washington, DC, USA, 1998; Volume 1.
25. Fajfar, P. Capacity spectrum method based on inelastic demand spectra. *Earthq. Eng. Struct. Dyn.* **1999**, *28*, 979–993. [CrossRef]
26. Freeman, S.A. Development and use of capacity spectrum method. In Proceedings of the 6th US National Conference on Earthquake Engineering, Seattle, WA, USA, 31 May–4 June 1998.
27. Milutinovic, Z.V.; Trendafiloski, G.S. *WP4: Level 2 Methodology—Code Based Approach, Case Study: Aseismic Design Codes in Macedonia*; RISK-UE WP4 L2 Report; IZIIS: Skopje, North Macedonia, 2002.

28. Vidic, T.; Fajfar, P.; Fischinger, M. Consistent inelastic design spectra: Strength and displacement. *Earthq. Eng. Struct. Dyn.* **1994**, *23*, 507–521. [CrossRef]
29. Fajfar, P. A nonlinear analysis method for performance-based seismic design. *Earthq. Spectra* **2000**, *16*, 573–592. [CrossRef]
30. Mahaney, J.A.; Paret, T.F.; Kehoe, B.E.; Freeman, S.A. The capacity spectrum method for evaluating structural response during the Loma Prieta earthquake. In Proceedings of the 1993 National Earthquake Conference, Memphis, TN, USA, 2–5 May 1993.
31. Department of Homeland Security, FEMA. *Multi-Hazard Loss Estimation Methodology: Earthquake Model*; Technical Report; Department of Homeland Security, FEMA: Washington, DC, USA, 2003.
32. Palanci, M.; Kalkan, A.; Sene, S.M. Investigation of shear effects on the capacity and demand estimation of RC buildings. *Struct. Eng. Mech.* **2016**, *60*, 1021–1038. [CrossRef]